Adsorption Conformation and Lateral Registry of Cobalt Porphines on Cu(111)

Journal:	*The Journal of Physical Chemistry*
Manuscript ID	Draft
Manuscript Type:	Article
Date Submitted by the Author:	n/a
Complete List of Authors:	Schwarz, Martin; Technical University of Munich, Department of Physics Garnica, Manuela; Technical University of Munich, Department of Physics Duncan, David; Diamond Light Source Ltd, Pérez Paz, Alejandro; Universidad del País Vasco UPV/EHU, Departamento de Física de Materiales; Yachay Tech University, School of Chemical Sciences and Engineering, School of Physical Sciences and Nanotechnology Ducke, Jacob; Technical University of Munich, Department of Physics Deimel, Peter; Technical University of Munich, Department of Physics Thakur, Pardeep Kumar; Diamond Light Source Lee, Tien-Lin; Diamond Light Source Rubio, Angel; Max-Planck-Institut fur Struktur und Dynamik der Materie; University of Hamburg, Center of Free-Electron Laser Science and Department of Physics; Universidad del País Vasco UPV/EHU, Departamento de Física de Materiales Barth, Johannes; Technical University of Munich, Department of Physics Allegretti, Francesco; Technical University of Munich, Department of Physics Auwärter, Willi; Technical University of Munich, Department of Physics

Adsorption Conformation and Lateral Registry of Cobalt Porphines on Cu(111)

Martin Schwarz[1], Manuela Garnica[1], David A. Duncan[2], Alejandro Pérez Paz[3,4], Jacob Ducke[1], Peter S. Deimel[1], Pardeep K. Thakur[2], Tien-Lin Lee[2], Angel Rubio[3,5,6], Johannes V. Barth[1], Francesco Allegretti[1], Willi Auwärter[1]*

[1]*Technical University of Munich, Department of Physics, 85748 Garching, Germany.*

[2]*Diamond Light Source, Harwell Science and Innovation Campus, Didcot, OX11 0DE, United Kingdom.*

[3]*Nano-Bio Spectroscopy Group and ETSF, Universidad del País Vasco, 20018 San Sebastián, Spain*

[4]*School of Chemical Sciences and Engineering, School of Physical Sciences and Nanotechnology, Yachay Tech University, Urcuquí 100119, Ecuador*

[5]*Max Planck Institute for the Structure and Dynamics of Matter, Luruper Chaussee 149, 22761 Hamburg, Germany*

[6]*Center for Free-Electron Laser Science & Department of Physics, University of Hamburg, Luruper Chaussee 149, 22761 Hamburg, Germany*

Abstract

The tetrapyrrole macrocycle of porphine is the common core of all porphyrin molecules, an interesting class of π-conjugated molecules with relevance in natural and artificial systems. The functionality of porphines on a solid surface can be tailored by the central metal atom and its interaction with the substrate. In this study, we present a local adsorption geometry determination for cobalt porphine on Cu(111) by means of complementary scanning tunneling microscopy, high-resolution X-ray photoelectron spectroscopy and X-ray standing wave measurements, and density functional theory calculations. Specifically, the Co center was determined to be at an adsorption height of 2.25 ± 0.04 Å occupying a bridge site. The macrocycle adopts a moderate asymmetric saddle-shape conformation, with the two pyrrole groups that are aligned perpendicular to the densely packed direction of the Cu(111) surface tilted away from the surface plane.

Introduction

Transition metal complexes hold great promise for technological and medical applications such as in photonic and optoelectronic devices,[1] catalysts,[2] and metal-based pharmaceuticals.[3,4] For instance, the metal ions in these molecules can be tailored such that they bind to a desired biomolecular target acting as a potential therapeutic agent,[5] and as a catalyst they offer control over the active site and its selectivity.[6,7] Frequently the applications require the organization of the metal complexes on a solid surface, whereby the interaction between the coordinated metal ion and the surface can drastically affect the functional properties of the complexes themselves. Consequently, a detailed understanding of the interfacial interactions between the complexes and the support is important for future integration of these molecular systems in functional nanodevices.[8,9] Tetrapyrroles, *e.g.* metalloporphyrins and metallophthalocyanines, are an important class of metal complexes due to their high stability, structural versatility, promising electronic properties and tunable molecular functionality.[10,11] The adsorption of these molecules on coinage metal surfaces has provided a rich playground for the engineering of complex nanoarchitectures by self-assembly and for understanding the reactivity and electronic structure of metal-organic interfaces.[12–14] Moreover, the conformation of the molecule can be altered significantly by the interaction with the metal substrate, thus resulting in changes of the intrinsic molecular properties.[15]

In recent years, different combined experimental and theoretical studies were devoted to determine the adsorption geometry of organic molecules[16–25] and in particular porphyrins on various substrates.[26–33] Specifically, Bürker *et al.* have studied the vertical height variation of functionalized porphyrins on Cu(111) upon copper metalation by means of

the X-ray standing wave (XSW) method.[34] They observed that the two inequivalent N atoms in tetra-phenyl porphyrin (TPP), adsorb at a height of 2.02 ± 0.08 Å and 2.23 ± 0.05 Å, prior to metalation while after metalation only one N species at 2.25 ± 0.02 Å was found. However no insight into the lateral registry was obtained. Furthermore, prior studies indicate that the lateral phenyl substituents of TPP can exert a significant influence on the final conformation of the molecule .[35,36] Additionally, due to an overwhelming signal from the bulk, metalation with atoms of the substrate hampers the determination of the vertical position of the porphyrin metal centers, which, as it is the active site of the molecule, is of fundamental interest in, *e.g.,* the ligation of adducts,[37] and the stacking behavior of multilayer systems.

The free-base porphine (2H-P) consists of four pyrrole rings connected by four methine (=C-) bridges forming an aromatic heterocyclic macrocycle and constitutes the base-unit of all porphyrinic nanosystems. Its central pocket can host a wide range of atoms including, but not limited to, lanthanides and transition metals, thus offering a vast playground to modify the functionality of the molecule.[13,14,38] Along with changes of the physical, chemical and optoelectronic properties,[39] the conformation can also be altered considerably.[33,36] In order to understand the molecule-substrate interactions of the base-unit porphine, a proper knowledge of the exact adsorption geometry is of fundamental interest. Bischoff *et al.* suggested a bridge adsorption site for 2H-P on Ag(111) based on the molecular orientations and the intermolecular spacing observed in STM.[40] For 2H-P/Cu(111), density functional theory (DFT) calculations predicted an average adsorption height of 2.40 Å at the bridge site, accompanied by a structural deformation of the molecule due to different interaction strengths of the nitrogen species with the substrate atoms.[26]

Herein, we report the experimental determination of the adsorption site and conformation of cobalt porphine (Co-P) on Cu(111). To this end, we conducted XSW experiments complemented by high-resolution X-ray photoelectron spectroscopy (HR-XPS) to measure the vertical height of Co-P on the Cu(111) surface, as well as to directly triangulate the lateral registry of the metal center. The capability of the XSW technique to resolve the substrate bonding of organic molecules has been reliably demonstrated in the last decade.[19,20,22,34,41] Scanning tunneling microscopy (STM) measurements of sub-monolayer Co-P were utilized to rule out the presence of multiple lateral adsorption sites and the molecular registry of Co-P, co-adsorbed with carbon monoxide (CO), was directly probed by this technique to confirm the XSW results on the single molecule level. The results of both experiments are interpreted and corroborated by density functional theory (DFT) calculations with van der Waals corrections.

Experimental and Computational Methods

Experimental Details

The HR-XPS and XSW measurements were conducted at Diamond Light Source at the end station of the I09 beamline with a base pressure of ~4×10^{-10} mbar. A Cu(111) single crystal was cleaned by repeated sputtering and annealing cycles. The Co-P molecules (purchased from Frontier Scientific, purity 95%) were degassed thoroughly and evaporated from a home-built quartz crucible evaporator at a temperature of 600 K while the sample was kept at room temperature. The final molecular coverage (~20% of a monolayer, comparable to the STM image shown in Figure 1a) was calculated using the intensity ratio of the cross-section corrected C 1s to Cu 3p core-level peaks

measured at the same photon energy and the unit cell size of a Co-P molecule.[40] The C 1s and N 1s core levels were acquired using a photon energy of 641 eV, the Co 2p core-level spectra with a photon energy of 2400 eV. XP survey spectra, taken over a wide range of binding energies, showed no components other than the expected C, N, Co and Cu features. The binding energy scale of the C 1s, N 1s and Co 2p spectra was calibrated against the Cu 3p core level measured at the same photon energy and assumed to be at a binding energy of 75.14 eV.[42]

For the XSW measurements, the X-ray beam was defocused to approximately 400×400 μm^2 and stepped over the sample such that each XSW profile was acquired at a different sample position. To further avoid beam damage, the beam intensity was reduced to 20% by detuning the undulator. Possible beam damage was monitored by comparing the C 1s and N 1s core-level spectra before and after each XSW measurement, where no changes were detected. The hemispherical electron analyzer, a VG Scienta EW4000 HAXPES with an acceptance angle of ±28°, was mounted with an angle of 90° with respect to the incident synchrotron light and the center of its angular acceptance in the plane of the photon polarization. The XSW scans were obtained from the (111) and $(1\bar{1}1)$ Bragg reflection of Cu (E_{Bragg} ~2972 eV at 300 K with a Bragg angle of ~90°). The intensity of the crystal Bragg reflection was measured, simultaneously to the absorption profiles (acquired from core-level photoemission yields), via a fluorescent screen mounted on the port of the incident X-ray beam by means of a CCD camera. Prior to each XSW measurement a reflectivity curve was acquired to determine the Bragg energy at a given position on the sample, and the subsequent XSW measurement was acquired across a window of ±5 eV around that energy. In total, 16 distinct sample spots were used for the measurements, resulting in four individual XSW spectra for

C 1s, N 1s and Co 2p at the (111) Bragg reflection and additional four Co 2p spectra at the $(1\bar{1}1)$ Bragg reflection. The respective XP spectra were then averaged in order to improve the signal to noise ratio. The C 1s and N 1s spectra were fitted with Voigt profiles (convolution of a Gaussian and a Lorentzian), while Co 2p spectra were fitted with a convolution of an asymmetric Doniach-Šunjić line shape and a Gaussian profile. Integrated intensities of the core-level peaks were used to obtain the relative X-ray absorption rate. Non-dipolar corrections were applied according to Ref. [43]. An angle θ = 18° [15°], as defined in Ref. [43], was used for the XSW measurements using the (111) [$(1\bar{1}1)$] Bragg reflection, respectively, and only photoemission corresponding to positive angles, emission angles that lay between the photon incidence direction and the photon polarization direction, were included in the fitting. All the XPS and XSW measurements were carried out at room temperature.

Analysis of the XSW measurement, utilizing dynamical theory, yields two structural parameters, the coherent position ($p^{111}/p^{1\bar{1}1}$) and the coherent fraction ($f^{111}/f^{1\bar{1}1}$). In the case of the (111) reflection, for the Cu(111) substrate, the coherent position can be related to the average adsorption height $\bar{h} = (n + p^{111}) \cdot d_{111}$, with d_{111} = 2.087 Å being the layer spacing of Cu(111) and *n* an integer. The coherent fraction quantifies the level of order in the system, often equivalent to the fractional occupation of the adsorption site, and can vary within the range $0 \leq f^{111}, f^{1\bar{1}1} \leq 1$. A detailed description of the XSW method can be found in literature.[44]

The STM experiments were performed in a custom-designed ultra-high vacuum (UHV) chamber housing a CreaTec STM operated at 5 K. The base pressure during the experiment was $<5 \times 10^{-10}$ mbar. CO was deposited onto the Cu(111) sample surface

at sample temperatures below 15 K. All STM images were recorded in constant-current mode using an electrochemically etched tungsten tip. The WsXM software was used to process the STM data.[45]

Computational Details

Density functional theory (DFT) slab calculations were performed using the projector augmented wave pseudo-potential method[46] as implemented in the VASP code (version 5.4.1).[47–50] The PBE exchange-correlation functional was used in all calculations[51] and included van der Waals (vdW) corrections via the Tkatchenko-Scheffler approach.[52] The convergence threshold of the electronic cycle was set to 10^{-5} eV and a Gaussian smearing of 0.1 eV was used. All geometry optimizations used a kinetic energy cutoff of 400 eV. Calculations with higher cutoff (500 eV) show negligible variations in the results. A converged 5x5x1 Monkhorst-Pack k-point mesh and "PREC=accurate" settings in VASP were employed. The Cu(111) surface was modeled with the coordinates derived from a typical PBE lattice constant of 3.63 Å.[26,53] The low adsorbate coverage limit was investigated via an 8x8x4 Cu(111) slab that features a lateral porphine separation of 20.534 Å between Co centers. The Co-P was initially positioned with opposite N atoms along the bridge position of Cu(111),[54] which is similar to the adsorption mode of 2H-P/Cu(111) reported by Müller *et al.*,[26] that places the 2 amino groups N-H along the long bridge site. Other symmetry sites were also tested. The adsorbate and the two uppermost Cu layers were relaxed until all ionic forces were below 0.025 eV/Å. An 18 Å vacuum slab and dipole corrections were used to decouple the periodic images along the normal z direction. Spin polarized calculations were used for the isolated gas phase Co-P species yielding a net magnetic moment of 1.0 μ_B

localized on the $3d_{z^2}$ Co atomic orbital. The charge transfers were computed via the Bader analysis code.[55–57] STM images were simulated using the CP2K code[58] under several tip-wave (s, p_x, p_y) Tersoff-Hamann approximations.[59]

Results

HR-XPS data and analysis

The XPS experiments were conducted with a molecular coverage comparable to the STM image shown in Figure 1a. Figures 1b-d display high-resolution X-ray C 1s, N 1s and Co 2p core-level spectra of Co-P/Cu(111), whose fit parameters are summarized in Table 1. In the C 1s core-level spectrum (Figure 1b), two clearly distinct components with binding energies (E_b) of 284.8 eV and 284.0 eV can be distinguished. The component at higher binding energy stems from the eight carbon atoms directly bound to nitrogen atoms (C-N), while the lower binding energy component originates from the 12 carbon atoms that are bonded to only other carbon atoms (C-C).[25,35] The intensity ratio of the two peaks, 0.76, is in good agreement with the expected value of 0.67 (= 8/12). An additional comparatively weak component at E_b = 285.6 eV is tentatively assigned to a shake-up satellite, whereas the feature at E_b = 282.9 eV is most likely due to a minor amount of adventitious carbon on the surface of the crystal.

The N 1s photoemission spectrum (Figure 1c) shows a dominant peak at 398.6 eV with a small shoulder at higher binding energy (399.6 eV). An additional shoulder on the low binding energy side (398.3 eV) is identified by the curve-fitting analysis. The main peak is associated with nitrogen atoms bound to cobalt atoms (N-Co), while the shoulders are assigned to pyrrolic (-NH-) and iminic (=N-) nitrogen atoms of free-base porphine (2H-P)

molecules that are present as impurities from the Co-P powder. The area ratio of about 17:1 is in accordance with the nominal purity. The binding energy of the main peak is in good agreement with values reported for metalloporphyrins on surfaces in literature.[35,60–63]

The Co $2p_{3/2}$ core level (Figure 1d) exhibits a more complex line shape associated with the multiplet structure resulting from the open-shell character of the Co ion and is consistent with earlier reports on similar porphyrins.[37,60,64–66] The main peak is found at a binding energy of 778.2 eV, in good agreement with these previous studies of cobalt porphyrins on surfaces,[37,64–66] and the satellite feature at high binding energy is assigned to the unpaired electron in the *d* shell and its coupling to the core hole created in the *p* shell of the Co ion upon photoemission.[64,65]

Table 1 – XPS Fit Parameters for the Atomic Species of Co-P/Cu(111).[a]

Core level	E_b^0 (eV)	Γ (eV)	σ (eV)
C 1s (C-C)	284.0	0.12	0.69
C 1s (C-N)	284.8	0.12	0.53
N 1s	398.6	0.11	0.58
Co $2p_{3/2}$	778.2	0.31	0.55

[a] Peak position E_b^0, Lorentzian width Γ and Gaussian width σ obtained from the fits for the indicated components. Voigt line shapes are used for the curve-fitting of the C 1s and N 1s core level spectra, while a Doniach-Šunjić line shape was used to model the Co $2p_{3/2}$ line.

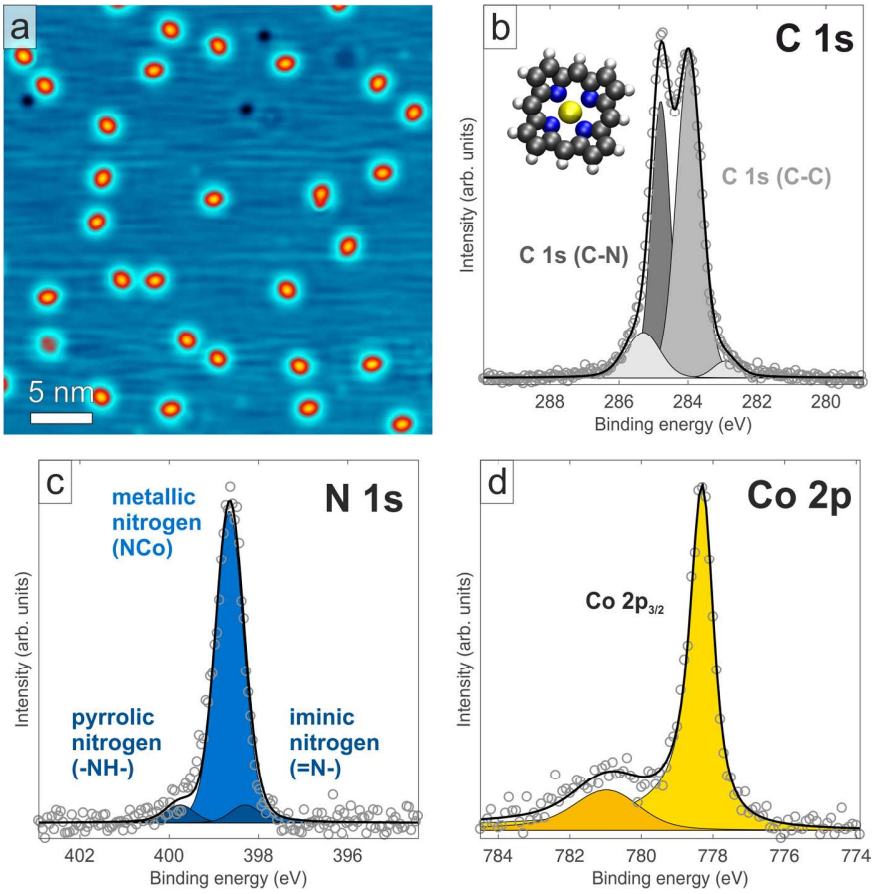

Figure 1 - (a) STM image showing a low coverage of Co-P/Cu(111). Scan parameters: U_b = -0.65 V, I_t = 230 pA. Corresponding high-resolution XP spectra of (b) C 1s, (c) N 1s, and (d) Co $2p_{3/2}$ core levels, respectively. Data points are background subtracted with a Shirley background. The colored areas are fits of the indicated components and the solid black line is the global fit. The inset in (b) shows a ball model of the Co-P molecule (gray: carbon, blue: nitrogen, yellow: cobalt, white: hydrogen).

XSW data and analysis

The results of the XSW measurements performed in a normal-incidence geometry with respect to the (111) Bragg reflection are displayed in Figure 2. A qualitative inspection shows that all absorption profiles exhibit a maximum around 1 eV above the Bragg energy, suggesting that the mean adsorption height of each species is largely similar, however, the more distant the atom is from the center of the molecule, the lower the

obtained coherent fraction is, as can be explained by the STM and DFT data discussed below. Quantitative analysis of the Co $2p_{3/2}$ absorption curve yields a very high coherent fraction, f^{111} = 0.90 ± 0.05, and a coherent position of p^{111} = 0.08 ± 0.03, which, assuming the adsorption height lies between the first and the second Cu(111) layer spacing projected above the surface, translates into an average adsorption height $\overline{h}$ = 2.25 ± 0.04 Å. The high coherent fraction indicates a well-defined adsorption height for all the molecules, and might also point to a well-defined adsorption site in terms of the lateral registry. For nitrogen a coherent fraction of f^{111} = 0.78 ± 0.03 and an average adsorption height $\overline{h}$ = 2.33 ± 0.06 Å are determined; for the carbon data, the C-N (C-C) species exhibits a coherent fraction f^{111} = 0.61 ± 0.04 (0.30 ± 0.06) and an average adsorption height of $\overline{h}$ = 2.37 ± 0.05 (2.44 ± 0.09) Å. The structural parameters are summarized in Table 2.

In order to determine the exact lateral adsorption site of the Co-P molecules, triangulation measurements[67,68] were conducted for the Co $2p_{3/2}$ core level utilizing the $(1\bar{1}1)$ Bragg reflection (see Supporting Information, Figure S1). The best fit of the relative absorption of the Co $2p_{3/2}$ core level yields a coherent fraction of $f^{1\bar{1}1}$ = 0.50 ± 0.06 and a coherent position of $p^{1\bar{1}1}$ = 0.91 ± 0.03. Considering different lateral positions above the close-packed surface and assuming a single site adsorption model for cobalt, triangulation calculations by refinement, which take into account the coherent fractions and positions of both Bragg reflections (see Figure S2), indicate that the measured data can only be reconciled with adsorption in a bridge site. This site would be expected to have a $f^{1\bar{1}1}$ = 0.33 (see eq. 4 in the Supporting Information and Ref. [44]), suggesting that the adsorption site might be slightly off the ideal bridge site. However, the higher

coherent fraction is more likely the result of the previously observed positive non-linearity in the EW4000 analyzer.[69] This latter interpretation is further reinforced by the quality of the fit being poor when the absorption rate is at its maximum (at around 1 eV in Figure S1), suggestive that the experimental count rate is approaching the saturation rate of the detector and thus the fit curve overreaches the experimental data.

The experimentally determined adsorption heights are in excellent agreement with the ones theoretically obtained from calculations with a well-considered set of functionals (see Table 2 and discussion below). Notably, the calculated heights are within 0.15 Å of the experimental values and lie well within the experimental uncertainty for the Co species. Importantly, the DFT calculations predict that the Co atom is located closest to the surface at a vertical distance of 2.29 Å. Moreover, the DFT results reveal adsorption centered over a bridge site and a distortion of the molecule (discussed later) that qualitatively matches the experimentally measured trend in coherent positions and is further corroborated by the observations in STM measurements.

Table 2 – Structural parameters obtained from the XSW analysis compared to the vertical distances calculated by DFT.[a]

	XSW – (111) Bragg reflection			**DFT**	**DFT**
	f^{111}	p^{111}	Adsorption height $\overline{h}$ (Å)	Calculated adsorption height $\overline{h}_0$ (Å)	XSW geometric factor a_{111}
C 1s (C-C)	0.30 ± 0.06	0.17 ± 0.05	2.44 ± 0.09	2.56	0.79
C 1s (C-N)	0.60 ± 0.04	0.14 ± 0.03	2.37 ± 0.05	2.50	0.93
N 1s	0.79 ± 0.03	0.12 ± 0.03	2.33 ± 0.06	2.42	0.98
Co 2p	0.90 ± 0.05	0.08 ± 0.02	2.25 ± 0.04	2.29	
	XSW – $(1\bar{1}1)$ Bragg reflection				
	$f^{1\bar{1}1}$	$p^{1\bar{1}1}$	Adsorption height $\overline{h}$ (Å)		
Co 2p	0.50 ± 0.06	0.91 ± 0.03	-		

[a] The XSW data obtained from the (111) Bragg reflection comprises the coherent fraction f^{111}, the coherent position p^{111}, and the corresponding mean adsorption height on bulk-extrapolated Cu(111) Bragg plane for the different atomic species of Co-P. Calculated vertical distances from DFT and the resulting geometric factor a_{111} are given for comparison. The XSW data obtained from the Co 2p core level using the $(1\bar{1}1)$ Bragg reflection (see Figure S1) comprise the coherent fraction $f^{1\bar{1}1}$, and the coherent position $p^{1\bar{1}1}$.

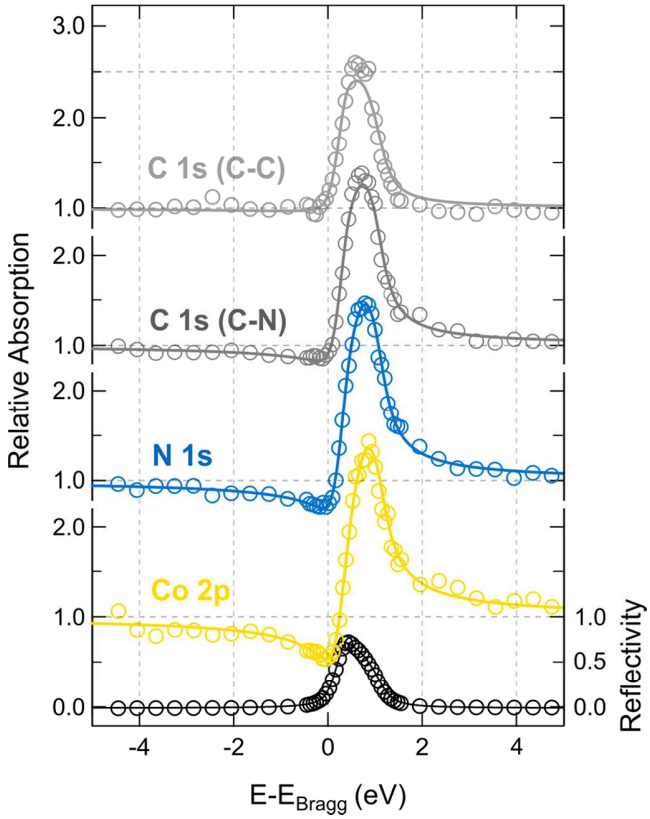

Figure 2 – Normal-incidence XSW absorption profiles of C 1s, N 1s and Co $2p_{3/2}$ of Co-P on Cu(111) at the (111) Bragg reflection. Solid lines are fits to the data. Black data points are the reflectivity curve.

STM data and analysis

At low coverage, dispersed Co-P are observed on the Cu(111) surface (see large-scale image in Figure 1a). Figure 3a displays the three orientations of Co-P/Cu(111) corresponding to the three-fold symmetry of the substrate: the two molecular axes (black dashed and solid lines in Figure 3b) are aligned along the $\langle 1\bar{1}0 \rangle$ and $\langle 11\bar{2} \rangle$ directions, respectively, of the underlying substrate. Specifically, the black dashed axis that corresponds to the weaker contrast of the molecule in the STM image, lies along one of the three equivalent densely packed $\langle 1\bar{1}0 \rangle$ directions of the substrate. Molecular rotation could be induced by the scanning STM tip (see Figure S3), but only resulted in aligning

the molecule along one of the other symmetrically equivalent directions. The bright contrast along one of the axes and the twofold symmetry of the molecule are observed for both positive and negative bias voltages (see Figure S4), and is largely independent of the shape and nature of the tip (see Figure S5), as discussed in detail below.

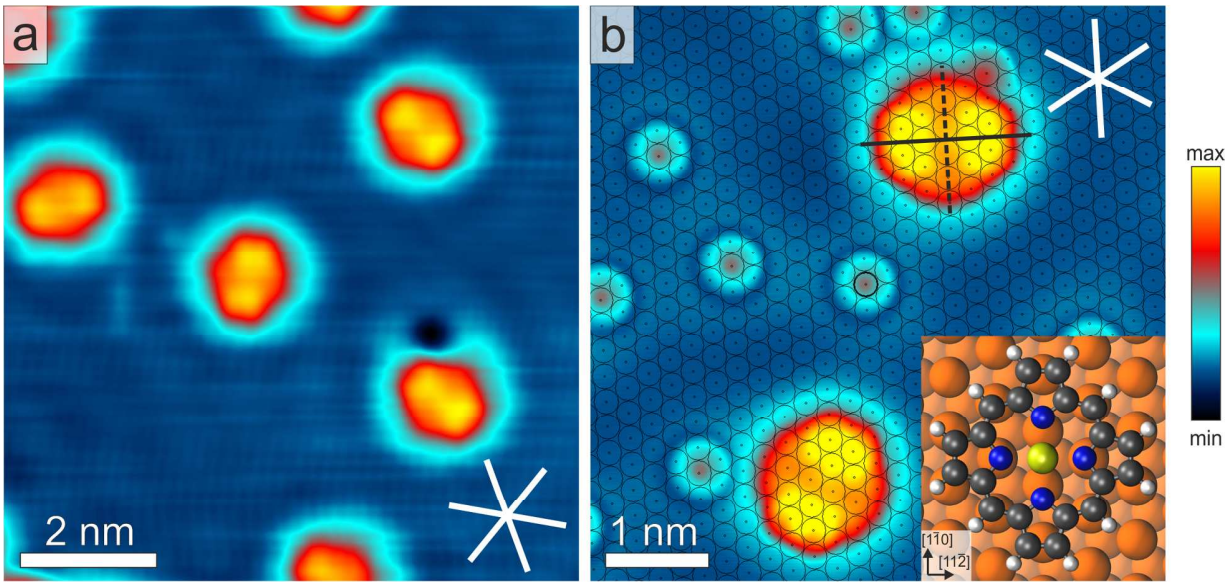

Figure 3 – STM images showing the adsorption geometry of Co-P/Cu(111). (a) The Co-P molecules adopt three different orientations where one molecular axis (see black dashed line in Figure 3b) is aligned with one of the three principal directions of the crystal (close-packed rows, white lines). The bright features of the Co-P molecules are aligned with the long bridge direction of the Cu(111) substrate. (b) Close-up view of two Co-P molecules together with CO molecules, which adsorb preferentially on atop sites. The atomic lattice is superimposed according to the CO adsorption sites. This clearly reveals that the Co atom in the center of the Co-P is located on bridge positions. The inset shows a top view of the relaxed adsorption geometry by DFT. Co, C, N and H atoms are depicted by the yellow, gray, blue, and white spheres, respectively. Scan parameters in (a): U_b = -0.5 V, I_t = 680 pA; in (b) U_b = 0.5 V, I_t = 800 pA.

To determine the adsorption site, CO molecules were deposited *in-situ* and used as markers, as CO is known to adsorb on atop sites on Cu(111) at low coverage at this particular temperature.[33,70] The CO showed no discernible interaction with the Co-P molecules, suggesting that the molecules do not affect the other's adsorption site. We

exploit the enhanced sub-molecular resolution obtained with CO-functionalized STM tips,[71] together with the atomic substrate lattice defined by the CO molecules, to determine the exact registry of the Co-P on the surface (Figure 3b). The image clearly reveals that the center of the Co-P molecules, and thus the Co atoms are exclusively located on bridge positions of the substrate, as predicted by the DFT calculations, and determined by the XSW measurements.

DFT calculations

The DFT calculations yield an adsorption energy of -4.80 eV for Co-P adsorption in bridge site (see inset Figure 3b). It should be noted that the adsorption energy obtained from DFT without vdW corrections is only -0.25 eV (*i.e.* the vdW stabilization contribution to the adsorption energy is large for Co-P/Cu(111): -4.55 eV). The Co-P macrocycle is bent along the $\langle 11\bar{2} \rangle$ direction while nearly flat along the $\langle 1\bar{1}0 \rangle$ direction (see Figure 4), reflecting an asymmetric saddle-shape-like conformation.

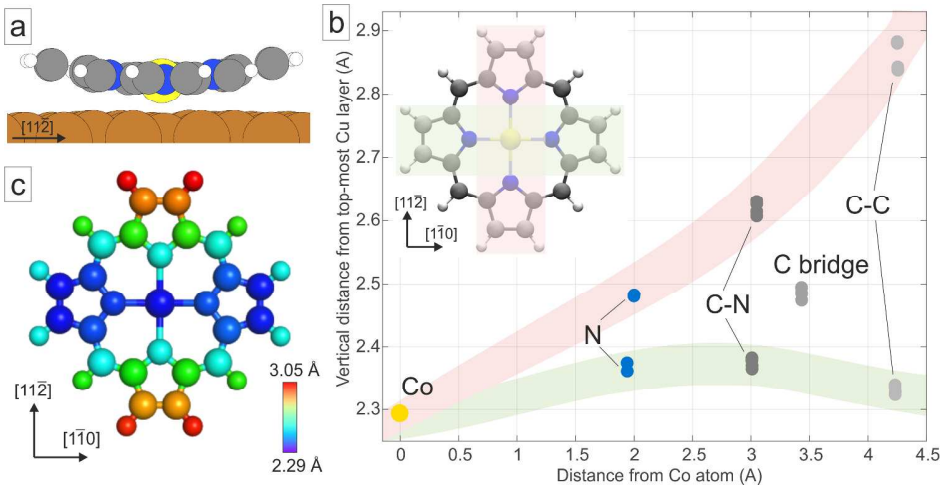

Figure 4 – Structural conformation predicted by the DFT calculations. In the most stable adsorption geometry of Co-P on Cu(111), the central cobalt atom (yellow) is located on a surface bridge site of the Cu substrate. (a) Side-view of the molecular model showing an asymmetric saddle-shape-like conformation

(the porphine macrocycle is bent upwards along the $\langle 11\bar{2} \rangle$ direction). (b) The Co-P molecule has two molecular axes, marked red and green in the inset. The carbon and nitrogen atoms along the main axis (red shaded) show an increased vertical position compared to the atoms along the second axis (shaded in green). (c) Color-coded plot indicating the adsorption height of each atom in the Co-P with respect to the mean top layer of Cu(111).

Calculations starting with the Co-P placed such that Co is on other high-symmetry sites (*e.g.* hcp hollow site) result in the molecule hopping back to the bridge site. Thus, we conclude that the bridge site is the global energy minimum. The Co atom, which lies above the bridge site, has a predicted adsorption height of 2.29 Å, corresponding to a Co-Cu bond length of 2.65 Å. The favored bridge adsorption geometry gives rise to two pairs of distinct nitrogen atoms (see inset of Figure 3b): The first pair are positioned along the short bridge direction, which is one of the densely packed $\langle 1\bar{1}0 \rangle$ directions of the crystal. This pair of N atoms are located off-atop, with an adsorption height, above the mean height of the outermost Cu layer, of 2.48 Å and a bond length of its nearest-neighbor (nn) Cu atom also of 2.48 Å (due to a subtle outward relaxation of the nn Cu atom). The N-Co bond length was predicted to be 1.95 Å (compared to 1.97 Å calculated for Co-P in gas phase). The second pair of N atoms are aligned along the long bridge direction (*i.e.* the $\langle 11\bar{2} \rangle$ directions of the crystal) in a near atop site, with a slightly decreased adsorption height (2.37 Å) above the outermost Cu layer, and a N-Cu bond length of 2.52 Å. The N-Co bond length was found to be slightly longer at 2.01 Å. A favored bridge adsorption position has also been reported for Co-Pc on Cu(111).[54,72] Notably, an adsorption configuration with the Co-P molecule rotated by 90° was also found to be stable (adsorption energy: -4.73 eV, see Figure S6), although energetically

slightly less favorable by 0.07 eV. This adsorption structure (Figure S6) exhibits a saddle-shape conformation with the two pyrrole rings along the $\langle 1\bar{1}0 \rangle$ directions of the crystal sitting significantly higher above the surface, in contrast to the global energy minimum configuration shown above and the experimental STM data discussed next. Note that this local minima more likely conforms to an asymmetric pyrrole stretch mode, like that observed for (NO)Fe-TPP,[73] than an actual rotation of the molecule.

According to our Bader analysis, the Co-P molecule receives 0.66 e^- from the Cu(111) substrate. Upon adsorption, the N atoms keep almost the same Bader valence charge (a 0.03 e^- increase), while Co gets 0.24 e^-, C atoms get 0.72 e^-, and H atoms lose 0.33 e^- with respect to isolated gas-phase Co-P. Upon Co-P adsorption, the work function of the Cu(111) is predicted to decrease by 0.59 eV.

Comparison of experimental and DFT results

Simulated and measured STM images of an isolated Co-P molecule are shown in Figures 5. The simulated images were obtained from a DFT-optimized Co-P on an 8x8x4 slab of Cu(111) (see “Experimental and Computational Methods” for details). For tunneling into unoccupied states (U_b = 0.5 V, Figure 5a-c), the experimental STM image, recorded with a CO-functionalized tip, features two bright lobes on the macrocycle that are mirrored across one axis of the molecule. The corresponding simulated STM images correctly reproduces these lobes, however, as pointed out by Gross *et al.*,[74] contribution of a *p*-wave tip orbital (in our case the p_x) is required to mimic the CO-functionalized STM tip, and to reproduce the fine sub-structure with all details. Both, the experimental and the simulated images show no significant signal at the position of the Co atom. For tunneling from occupied states (U_b = -0.5 V, Figure new 5d-f), the STM image maps the

central Co atom as a bright protrusion, the global appearance being well reproduced by the simulated images. Similar findings have been reported for Co-Pc/Cu(111)[54] and Cu-P/Cu(111).[35]

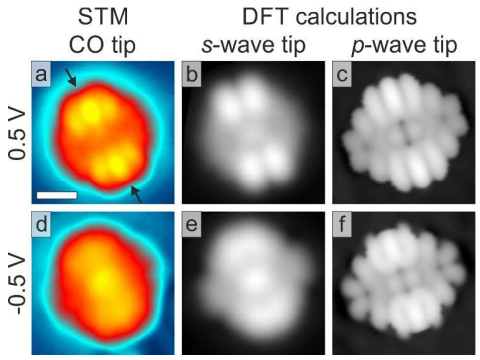

Figure 5 – Comparison between simulated and experimental STM images of Co-P on Cu(111). (a), (d) Experimental STM images of an individual Co-P molecule imaged with a CO-terminated tip displaying the unoccupied and the occupied states, respectively. The black arrows in (a) indicate the $\langle 11\bar{2} \rangle$ direction of the crystal. The corresponding simulated images from DFT using a *s*-wave tip (displayed in (b) and (e)), as well as a *p*-wave tip (displayed in (c) and (f)) are in good agreement with the experimental STM images. Specifically, the saddle-shape conformation is reproduced and the Co center becomes visible at negative bias voltage. Notably, p_x-wave tip orbitals are essential to mimic the 3-lobe fine structure observed in the experiment. Scan parameters in (a): U_b = 0.5 V, I_t = 800 pA; in (b) U_b = -0.5 V, I_t = 680 pA. Scale bar: 0.5 nm.

A side-view of the structural Co-P model is displayed in Figure 4a, indicating that the twofold geometry results in an asymmetric saddle-shape-like conformation with the pyrrole rings along the densely packed $\langle 11\bar{2} \rangle$ directions sitting significantly higher above the surface than those along the $\langle 1\bar{1}0 \rangle$ directions, with the macrocycle being rather flat along the latter direction (see Figure 4b). The significant difference in height between the spectroscopically inseparable species (~0.5 Å for the C-C species, see Figure 4c) aids to rationalize the significant decrease in coherent fraction observed in the XSW measurements. We want to point out, that the correlation between the strong contrast

observed in STM images and the geometric structure predicted by DFT is in line with previous reports on the structure of functionalized porphyrins.[75,76]

The vertical heights of the atomic species obtained by DFT were used to calculate geometric factors, a_{111} (one of three parameters that are used to model the coherent fraction – see Supporting Information and Refs. [44,77] for details), for the N, C-C and C-N species in the Co-P molecule (see Table 2). The geometric factors qualitatively model the experimentally measured trend in coherent fraction, however for all species the geometric factor is predicted to be too large to solely explain the observed coherent fractions (assuming an order factor of ~0.90, the coherent fraction observed for Co 2p). Were these predicted geometric factors correct, and if the order factor is indeed ~0.90, then, to explain the observed coherent fractions for the C-C species, a Debye-Waller factor (D-WF) of 0.43 would be required. Such a D-WF would correspond to a very large root mean square (rms) vibrational amplitude of 0.53 Å, and thus a Debye temperature of only ~100 K. It is unlikely that the C atoms would exhibit such an extreme vibrational amplitude, especially considering that the vibrational amplitude of the central Co atom must be significantly smaller. Another explanation for this quantitative disagreement may lie in the nature of the DFT calculations, which model the adsorption at 0 K, whereas the experiments were performed close to 300 K. Thus finite temperature effects[78] such as an adsorption potential of the pyrrole ring adsorbed along the $\langle 11\bar{2} \rangle$ directions that is strongly repulsive for small decreases in adsorption height, but weakly attractive for large increases, could well result in a significant change in the difference between in the mean adsorption of the two pairs of pyrrole rings.

Discussion

At low coverage, the adsorption of Co-P is driven by a repulsive intermolecular interaction, together with a strong molecule-substrate interaction. This is evidenced by the tendency of molecules to remain far apart from each other (Figure 1a) and is fully in line with previous studies that have shown sub-monolayer coverages of porphine molecules resulting in isolated molecules on the Ag(111) and the Cu(111) surface.[35,40] Importantly, the determined adsorption geometry is therefore dominated by molecule-substrate interactions. Upon adsorption on the Cu(111) surface, the symmetry of the Co-P molecule is reduced from a fourfold D_{4h}-symmetry in gas phase to a two-fold symmetry on the surface. As demonstrated, a moderate asymmetric saddle-shape conformation contributes to this symmetry reduction. While geometric origins for the symmetry reduction on coinage metal surfaces could never be detected experimentally for porphines so far,[35,40] deformations have been reported for larger tetrapyrrole derivatives. In the case of Co-Pc[54] and Fe-Pc[79] on Cu(111) the deformation results in one of the molecular axes getting closer to the surface, whereas in the case of 2H-TPP on Cu(111)[36] or Co-TPP on Cu(110)[80] a more severe non-planar deformation is observed, revealing the conformational flexibility of these compounds.

The only single-site interpretation of the XSW triangulation compatible with the experimental results involves adsorption in a bridge site, which would have an expected $p_{theo}^{1\bar{1}1}$ = 0.86 (see Supporting Information for details) and $f_{theo}^{1\bar{1}1}$ = 0.33 · f_{exp}^{111},[44] compared to the experimental $p_{exp}^{1\bar{1}1}$ = 0.91 ± 0.03 and $f_{exp}^{1\bar{1}1}$ = 0.50 ± 0.06. As discussed above, though the measured coherent fraction is higher than would be expected, this effect is attributed to the detector non-linearity.[69] However, if a two-site model is considered, then

this coherent fraction and position would correspond to co-adsorption in hcp and fcc hollow sites. Such co-adsorption is clearly refuted by the STM measurements, which only observe three distinct orientations of the Co-P molecules. A mixture of hcp and fcc sites would necessitate the presence of six possible orientations, as the hcp site is a false mirror image of the fcc site. Furthermore, the analysis of the STM images, based on the well-known CO adsorption site on Cu(111) as well as the DFT prediction of the bridge site corroborate the single-site interpretation. The same adsorption site has been proposed for 2H-P as well as for other metal derivatives[33] on Cu(111) indicating that the Co-Cu interaction does not dictate the bridge adsorption site.

The binding energy of the Co $2p_{3/2}$ core-level peak was found to be 778.2 eV, which is more compatible with a Co(0) oxidation state (778.1 eV for Co metal[81]), than with the expected nominal oxidation state of +2 (780.0 eV for Co-TPP multilayer on silver [64]). This results from the pronounced different electronic environment between these systems (metal, molecular multilayer and molecular monolayer on a metal) and can be mostly explained by the differing abilities of each system to screen the core hole left by the photoemission process and are thus a final state effect, as observed on numerous porphine-based species on various substrates.[35,40,64,82] Thus, such final states effect on the binding energy can dominate the contribution from charge transfer. This is a strong reminder of the dangers to assigning oxidation state by simple inspection of binding energy. The significant overlap between the orbitals of the Co atom and the substrate, implied by the charge transfer, suggests that the primary local interaction between the substrate and the molecule is through the Co atom, thus its adsorption height markedly below the macrocycle. It is therefore likely that the Co-P would exhibit a significant

surface *trans*-effect.[25,83] Note also that the determined adsorption heights are reduced compared to the value of 2.40 Å reported for 2H-P/Cu(111) in DFT calculations.[26]

Furthermore, we were not able to resolve any signature of a Kondo resonance on the Co-P molecule by scanning tunneling spectroscopy (STS) experiments conducted with a metallic tip. Observation of a Kondo signal is possible when the unpaired electron of the magnetic adsorbate is neither too weakly nor too strongly coupled to the substrate electron bath.[25] It has been shown that switching of the Kondo effect in Co-tetra-pyridyl porphyrin (Co-TPyP) on Cu(111) can be controlled via intermolecular interactions.[84] In our case, the isolated gas-phase Co-P has a magnetic moment of 1.0 μ_B and a spin density clearly localized on the half-filled $3d_{z^2}$ orbital of the Co atom. However, upon adsorption, the $3d_{z^2}$ orbital of the Co atom interacts strongly with the Cu(111) substrate leading to a complete quenching of the magnetic moment of the Co-P. This assertion is in line with previous DFT calculations[54,85] and experimental studies[86] on Co-Pc/Cu(111) that also report a modification of the magnetic properties of the molecule upon adsorption.

Although the quenching of magnetic properties, the sizable charge transfer (0.66 e^-), and the large total adsorption energy (-4.80 eV) might suggest the Co-P molecules being strongly chemisorbed on the Cu(111) substrate, this interpretation has to be regarded with caution: in fact, vdW corrections result in a dramatic difference in the total adsorption energy (-4.55 eV compared to -0.25 eV without vdW correction).

Conclusions

In this work, we have determined the local adsorption geometry and the lateral registry of Co-P on Cu(111) with atomic precision. Most notably, the cobalt in the central pocket of the macrocycle is the closest atom to the surface, exclusively occupying a bridge site of the copper surface. The symmetry of this adsorption site is reflected in three equivalent molecular orientations observed by STM. The adsorption mode of Co-P molecules is mainly governed by vdW interactions, though some indications of chemical adsorption (short Co-Cu distance, large Bader charge transfer) are present. The Co center exhibits a significant interaction with the Cu(111) substrate, with a Co-Cu bond distance of 2.65 Å. The twofold symmetric appearance of the Co-P molecules is rationalized by an asymmetric deformation along the long bridge direction. This distortion, which was previously not recognized for porphines on coinage metals,[35,40,83,87] is less pronounced than in pyridyl-[33] and phenyl-functionalized porphyrins.[62,76,87–89] The knowledge of the geometric structure and the adsorption height of Co-P/Cu(111) is of fundamental relevance in order to understand the functionality of Co-P and related metal-organic complexes on surfaces.

Supporting Information

Additional STM, XSW and DFT data.

Competing financial interests

The authors declare no competing financial interests.

Corresponding Authors

* Willi Auwärter, Email: wau@tum.de

Acknowledgments

This work is supported by the European Research Council Consolidator Grant NanoSurfs (No. 615233) and the Munich-Center for Advanced Photonics (MAP). M.G. would like to acknowledge the H2020-MSCA-IF-2014 programme. W.A. acknowledges funding by the Deutsche Forschungsgemeinschaft via a Heisenberg professorship. A.P.P. acknowledges postdoctoral fellowship from the Spanish "Juan de la Cierva-incorporación" program (IJCI-2014-20147). We thank Diamond Light Source for the award of beam time and funding.

References

(1) Kalyanasundaram, K. Applications of Functionalized Transition Metal Complexes in Photonic and Optoelectronic Devices. *Coord. Chem. Rev.* **1998**, *177*, 347–414.

(2) Hartley, F. R. *Supported Metal Complexes: A New Generation of Catalysts*; Catalysis by Metal Complexes, 0920-4652 6; Springer Netherlands: Dordrecht, 1985.

(3) Che, C.-M.; Siu, F.-M. Metal Complexes in Medicine with a Focus on Enzyme Inhibition. *Curr. Opin. Chem. Biol.* **2010**, *14*, 255–261.

(4) Kilpin, K. J.; Dyson, P. J. Enzyme Inhibition by Metal Complexes: Concepts, Strategies and Applications. *Chem. Sci.* **2013**, *4*, 1410.

(5) Zhang, C. X.; Lippard, S. J. New Metal Complexes as Potential Therapeutics. *Curr. Opin. Chem. Biol.* **2003**, *7*, 481–489.

(6) Rogge, S. M. J.; Bavykina, A.; Hajek, J.; Garcia, H.; Olivos-Suarez, A. I.; Sepúlveda-Escribano, A.; Vimont, A.; Clet, G.; Bazin, P.; Kapteijn, F. *et al.* Metal-Organic and Covalent Organic Frameworks as Single-Site Catalysts. *Chem. Soc. Rev.* **2017**, *46*, 3134–3184.

(7) Thomas, J. M.; Raja, R.; Lewis, D. W. Single-Site Heterogeneous Catalysts. *Angew. Chem., Int. Ed. Engl.* **2005**, *44*, 6456–6482.

(8) Barth, J. V. Molecular Architectonic on Metal Surfaces. *Annu. Rev. Phys. Chem.* **2007**, *58*, 375–407.

(9) Koch, N. Organic Electronic Devices and their Functional Interfaces. *ChemPhysChem* **2007**, *8*, 1438–1455.

(10) Gottfried, J. M. Surface Chemistry of Porphyrins and Phthalocyanines. *Surf. Sci. Rep.* **2015**, *70*, 259–379.

(11) Kadish, K. M.; Smith, K. M.; Guilard, R. *The Porphyrin Handbook*; Academic Press: San Diego (Calif.), London, Sydney, 2003.

(12) Auwärter, W.; Écija, D.; Klappenberger, F.; Barth, J. V. Porphyrins at Interfaces. *Nat. Chem.* **2015**, *7*, 105–120.

(13) Auwärter, W.; Weber-Bargioni, A.; Brink, S.; Riemann, A.; Schiffrin, A.; Ruben, M.; Barth, J. V. Controlled Metalation of Self-Assembled Porphyrin Nanoarrays in Two Dimensions. *ChemPhysChem* **2007**, *8*, 250–254.

(14) Diller, K.; Papageorgiou, A. C.; Klappenberger, F.; Allegretti, F.; Barth, J. V.; Auwärter, W. In Vacuo Interfacial Tetrapyrrole Metallation. *Chem. Soc. Rev.* **2016**, *45*, 1629–1656.

(15) Rosei, F.; Schunack, M.; Naitoh, Y.; Jiang, P.; Gourdon, A.; Laegsgaard, E.; Stensgaard, I.; Joachim, C.; Besenbacher, F. Properties of Large Organic Molecules on Metal Surfaces. *Prog. Surf. Sci.* **2003**, *71*, 95–146.

(16) Schuler, B.; Liu, W.; Tkatchenko, A.; Moll, N.; Meyer, G.; Mistry, A.; Fox, D.; Gross, L. Adsorption Geometry Determination of Single Molecules by Atomic Force Microscopy. *Phys. Rev. Lett.* **2013**, *111*, 106103.

(17) Weiß, S.; Krieger, I.; Heepenstrick, T.; Soubatch, S.; Sokolowski, M.; Tautz, F. S. Determination of the Adsorption Geometry of PTCDA on the Cu(100) Surface. *Phys. Rev. B* **2017**, *96*, 75414.

(18) Baby, A.; Gruenewald, M.; Zwick, C.; Otto, F.; Forker, R.; van Straaten, G.; Franke, M.; Stadtmüller, B.; Kumpf, C.; Brivio, G. P. *et al.* Fully Atomistic Understanding of the Electronic and Optical Properties of a Prototypical Doped Charge-Transfer Interface. *ACS Nano* **2017**, *11*, 10495–10508.

(19) Kröger, I.; Stadtmüller, B.; Kumpf, C. Submonolayer and Multilayer Growth of Titaniumoxide-Phthalocyanine on Ag(111). *New J. Phys.* **2016**, *18*, 113022.

(20) Bürker, C.; Ferri, N.; Tkatchenko, A.; Gerlach, A.; Niederhausen, J.; Hosokai, T.; Duhm, S.; Zegenhagen, J.; Koch, N.; Schreiber, F. Exploring the Bonding of Large Hydrocarbons on Noble Metals: Diindoperylene on Cu(111), Ag(111), and Au(111). *Phys. Rev. B* **2013**, *87*, 165443.

(21) Mercurio, G.; Maurer, R. J.; Hagen, S.; Leyssner, F.; Meyer, J.; Tegeder, P.; Soubatch, S.; Reuter, K.; Tautz, F. S. X-ray Standing Wave Simulations Based on Fourier Vector Analysis as a Method to Retrieve Complex Molecular Adsorption Geometries. *Front. Physics* **2014**, *2,* DOI: 10.3389/fphy.2014.00002.

(22) Hauschild, A.; Karki, K.; Cowie, B. C. C.; Rohlfing, M.; Tautz, F. S.; Sokolowski, M. Molecular Distortions and Chemical Bonding of a Large π-Conjugated Molecule on a Metal Surface. *Phys. Rev. Lett.* **2005**, *94*, 36106.

(23) Gerlach, A.; Schreiber, F.; Sellner, S.; Dosch, H.; Vartanyants, I. A.; Cowie, B. C. C.; Lee, T.-L.; Zegenhagen, J. Adsorption-Induced Distortion of F_{16}CuPc on Cu(111) and Ag(111): An X-ray Standing Wave Study. *Phys. Rev. B* **2005**, *71*, 18.

(24) Wruss, E.; Hofmann, O. T.; Egger, D. A.; Verwüster, E.; Gerlach, A.; Schreiber, F.; Zojer, E. Adsorption Behavior of Nonplanar Phthalocyanines: Competition of Different Adsorption Conformations. *J. Phys. Chem. C* **2016**, *120*, 6869–6875.

(25) Deimel, P. S.; Bababrik, R. M.; Wang, B.; Blowey, P. J.; Rochford, L. A.; Thakur, P. K.; Lee, T.-L.; Bocquet, M.-L.; Barth, J. V.; Woodruff, D. P. *et al.* Direct Quantitative Identification of the "Surface Trans-Effect". *Chem. Sci.* **2016**, *7*, 5647–5656.

(26) Müller, M.; Diller, K.; Maurer, R. J.; Reuter, K. Interfacial Charge Rearrangement and Intermolecular Interactions: Density-Functional Theory Study of Free-Base Porphine Adsorbed on Ag(111) and Cu(111). *J. Chem. Phys.* **2016**, *144*, 24701.

(27) Leung, K.; Rempe, S. B.; Schultz, P. A.; Sproviero, E. M.; Batista, V. S.; Chandross, M. E.; Medforth, C. J. Density Functional Theory and DFT+U Study of Transition Metal Porphines Adsorbed on Au(111) Surfaces and Effects of Applied Electric Fields. *J. Am. Chem. Soc.* **2006**, *128*, 3659–3668.

(28) Zhang, L.; Lepper, M.; Stark, M.; Menzel, T.; Lungerich, D.; Jux, N.; Hieringer, W.; Steinrück, H.-P.; Marbach, H. On the Critical Role of the Substrate: The Adsorption Behaviour of Tetrabenzoporphyrins on Different Metal Surfaces. *Phys. Chem. Chem. Phys.* **2017**, *19*, 20281–20289.

(29) Lepper, M.; Köbl, J.; Schmitt, T.; Gurrath, M.; Siervo, A. de; Schneider, M. A.; Steinrück, H.-P.; Meyer, B.; Marbach, H.; Hieringer, W. Inverted Porphyrins: A Distorted Adsorption Geometry of Free-Base Porphyrins on Cu(111). *Chem. Commun.* **2017**, *53*, 8207–8210.

(30) Albrecht, F.; Bischoff, F.; Auwärter, W.; Barth, J. V.; Repp, J. Direct Identification and Determination of Conformational Response in Adsorbed Individual Nonplanar Molecular Species Using Noncontact Atomic Force Microscopy. *Nano Lett.* **2016**, *16*, 7703–7709.

(31) Dyer, M. S.; Robin, A.; Haq, S.; Raval, R.; Persson, M.; Klimes, J. Understanding the Interaction of the Porphyrin Macrocycle to Reactive Metal Substrates: Structure, Bonding, and Adatom Capture. *ACS Nano* **2011**, *5*, 1831–1838.

(32) Yokoyama, T.; Yokoyama, S.; Kamikado, T.; Mashiko, S. Nonplanar Adsorption and Orientational Ordering of Porphyrin Molecules on Au(111). *J. Chem. Phys.* **2001**, *115*, 3814–3818.

(33) Auwärter, W.; Klappenberger, F.; Weber-Bargioni, A.; Schiffrin, A.; Strunskus, T.; Wöll, C.; Pennec, Y.; Riemann, A.; Barth, J. V. Conformational Adaptation and Selective Adatom Capturing of Tetrapyridyl-Porphyrin Molecules on a Copper (111) Surface. *J. Am. Chem. Soc.* **2007**, *129*, 11279–11285.

(34) Bürker, C.; Franco-Cañellas, A.; Broch, K.; Lee, T.-L.; Gerlach, A.; Schreiber, F. Self-Metalation of 2H-Tetraphenylporphyrin on Cu(111) Studied with XSW: Influence of the Central Metal Atom on the Adsorption Distance. *J. Phys. Chem. C* **2014**, *118*, 13659–13666.

(35) Diller, K.; Klappenberger, F.; Allegretti, F.; Papageorgiou, A. C.; Fischer, S.; Wiengarten, A.; Joshi, S.; Seufert, K.; Écija, D.; Auwärter, W. *et al.* Investigating the Molecule-Substrate Interaction of Prototypic Tetrapyrrole Compounds: Adsorption and Self-Metalation of Porphine on Cu(111). *J. Chem. Phys.* **2013**, *138*, 154710-1-154710-9.

(36) Diller, K.; Klappenberger, F.; Marschall, M.; Hermann, K.; Nefedov, A.; Woll, C.; Barth, J. V. Self-Metalation of 2H-Tetraphenylporphyrin on Cu(111): an X-ray Spectroscopy Study. *J. Chem. Phys.* **2012**, *136*, 14705.

(37) Wäckerlin, C.; Chylarecka, D.; Kleibert, A.; Müller, K.; Iacovita, C.; Nolting, F.; Jung, T. A.; Ballav, N. Controlling Spins in Adsorbed Molecules by a Chemical Switch. *Nat. Commun.* **2010**, *1*, 61.

(38) Urgel, J. I.; Écija, D.; Auwärter, W.; Stassen, D.; Bonifazi, D.; Barth, J. V. Orthogonal Insertion of Lanthanide and Transition-Metal Atoms in Metal-Organic Networks on Surfaces. *Angew. Chem., Int. Ed. Engl.* **2015**, *54*, 6163–6167.

(39) Senge, M. O.; Fazekas, M.; Notaras, E. G. A.; Blau, W. J.; Zawadzka, M.; Locos, O. B.; Ni Mhuircheartaigh, E. M. Nonlinear Optical Properties of Porphyrins. *Adv. Mater.* **2007**, *19*, 2737–2774.

(40) Bischoff, F.; Seufert, K.; Auwärter, W.; Joshi, S.; Vijayaraghavan, S.; Écija, D.; Diller, K.; Papageorgiou, A. C.; Fischer, S.; Allegretti, F. *et al.* How Surface Bonding and Repulsive Interactions Cause Phase Transformations: Ordering of a Prototype Macrocyclic Compound on Ag(111). *ACS Nano* **2013**, *7*, 3139–3149.

(41) Kröger, I.; Stadtmüller, B.; Kleimann, C.; Rajput, P.; Kumpf, C. Normal-Incidence X-ray Standing-Wave Study of Copper Phthalocyanine Submonolayers on Cu(111) and Au(111). *Phys. Rev. B* **2011**, *83*, 195414.

(42) Seah, M. P.; Smith, G. C.; Anthony, M. T. AES: Energy Calibration of Electron Spectrometers. I - An Absolute, Traceable Energy Calibration and the Provision of Atomic Reference Line Energies. *Surf. Interface Anal.* **1990**, *15*, 293–308.

(43) Fisher, C. J.; Ithin, R.; Jones, R. G.; Jackson, G. J.; Woodruff, D. P.; Cowie, B. C. C. Non-Dipole Photoemission Effects in X-ray Standing Wavefield Determination of Surface Structure. *J. Phys. Cond. Matter* **1998**, *10*, L623-L629.

(44) Woodruff, D. P. Surface Structure Determination Using X-ray Standing Waves. *Rep. Prog. Phys.* **2005**, *68*, 743–798.

(45) Horcas, I.; Fernandez, R.; Gomez-Rodriguez, J. M.; Colchero, J.; Gomez-Herrero, J.; Baro, A. M. WSXM: A Software for Scanning Probe Microscopy and a Tool for Nanotechnology. *Rev. Sci. Instrum.* **2007**, *78*, 013705-1 - 013705-8.

(46) Blöchl, P. E. Projector Augmented-Wave Method. *Phys. Rev. B* **1994**, *50*, 17953–17979.

(47) Kresse, G.; Furthmüller, J. Efficient Iterative Schemes for Ab Initio Total-Energy Calculations Using a Plane-Wave Basis Set. *Phys. Rev. B* **1996**, *54*, 11169–11186.

(48) Kresse, G.; Hafner, J. Ab Initio Molecular Dynamics for Liquid Metals. *Phys. Rev. B* **1993**, *47*, 558–561.

(49) Kresse, G.; Hafner, J. Norm-Conserving and Ultrasoft Pseudopotentials for First-Row and Transition Elements. *J. Phys.: Condens. Matter* **1994**, *6*, 8245–8257.

(50) Kresse, G.; Joubert, D. From Ultrasoft Pseudopotentials to the Projector Augmented-Wave Method. *Phys. Rev. B* **1999**, *59*, 1758–1775.

(51) Perdew, J. P.; Burke, K.; Ernzerhof, M. Generalized Gradient Approximation Made Simple. *Phys. Rev. Lett.* **1996**, *77*, 3865–3868.

(52) Tkatchenko, A.; Scheffler, M. Accurate Molecular van der Waals Interactions from Ground-State Electron Density and Free-Atom Reference Data. *Phys. Rev. Lett.* **2009**, *102*, 73005.

(53) Koitz, R.; Seitsonen, A. P.; Iannuzzi, M.; Hutter, J. Structural and Electronic Properties of a Large-Scale Moire Pattern of Hexagonal Boron Nitride on Cu(111) Studied with Density Functional Theory. *Nanoscale* **2013**, *5*, 5589–5595.

(54) Cuadrado, R.; Cerda, J. I.; Wang, Y.; Xin, G.; Berndt, R.; Tang, H. CoPc Adsorption on Cu(111): Origin of the C4 to C2 Symmetry Reduction. *J. Chem. Phys.* **2010**, *133*, 154701-1-154701-7.

(55) Henkelman, G.; Arnaldsson, A.; Jónsson, H. A Fast and Robust Algorithm for Bader Decomposition of Charge Density. *Comput. Mater. Sci.* **2006**, *36*, 354–360.

(56) Sanville, E.; Kenny, S. D.; Smith, R.; Henkelman, G. Improved Grid-Based Algorithm for Bader Charge Allocation. *J. Comput. Chem.* **2007**, *28*, 899–908.

(57) Tang, W.; Sanville, E.; Henkelman, G. A Grid-Based Bader Analysis Algorithm Without Lattice Bias. *J. Phys.: Condens. Matter* **2009**, *21*, 84204.

(58) VandeVondele, J.; Krack, M.; Mohamed, F.; Parrinello, M.; Chassaing, T.; Hutter, J. Quickstep: Fast and Accurate Density Functional Calculations Using a Mixed Gaussian and Plane Waves Approach. *Comput. Phys. Commun.* **2005**, *167*, 103–128.

(59) Tersoff, J.; Hamann, D. R. Theory of the Scanning Tunneling Microscope. *Phys. Rev. B* **1985**, *31*, 805–813.

(60) Gottfried, J. M.; Flechtner, K.; Kretschmann, A.; Lukasczyk, T.; Steinrück, H.-P. Direct Synthesis of a Metalloporphyrin Complex on a Surface. *J. Am. Chem. Soc.* **2006**, *128*, 5644–5645.

(61) Niwa, Y.; Kobayashi, H.; Tsuchiya, T. X-ray Photoelectron Spectroscopy of Tetraphenylporphin and Phthalocyanine. *J. Chem. Phys.* **1974**, *60*, 799–807.

(62) Di Santo, G.; Castellarin-Cudia, C.; Fanetti, M.; Taleatu, B.; Borghetti, P.; Sangaletti, L.; Floreano, L.; Magnano, E.; Bondino, F.; Goldoni, A. Conformational Adaptation and Electronic Structure of 2H-Tetraphenylporphyrin on Ag(111) during Fe Metalation. *J. Phys. Chem. C* **2011**, *115*, 4155–4162.

(63) Scudiero, L.; Barlow, D. E.; Hipps, K. W. Physical Properties and Metal Ion Specific Scanning Tunneling Microscopy Images of Metal(II) Tetraphenylporphyrins Deposited from Vapor onto Gold (111). *J. Phys. Chem. B* **2000**, *104*, 11899–11905.

(64) Lukasczyk, T.; Flechtner, K.; Merte, L. R.; Jux, N.; Maier, F.; Gottfried, J. M.; Steinrück, H.-P. Interaction of Cobalt(II) Tetraarylporphyrins with a Ag(111) Surface Studied with Photoelectron Spectroscopy. *J. Phys. Chem. C* **2007**, *111*, 3090–3098.

(65) Flechtner, K.; Kretschmann, A.; Steinrück, H.-P.; Gottfried, J. M. NO-Induced Reversible Switching of the Electronic Interaction Between a Porphyrin-Coordinated Cobalt Ion and a Silver Surface. *J. Am. Chem. Soc.* **2007**, *129*, 12110–12111.

(66) Wechsler, D.; Franke, M.; Tariq, Q.; Zhang, L.; Lee, T.-L.; Thakur, P. K.; Tsud, N.; Bercha, S.; Prince, K. C.; Steinrück, H.-P. *et al.* Adsorption Structure of Cobalt Tetraphenylporphyrin on Ag(100). *J. Phys. Chem. C* **2017**, *121*, 5667–5674.

(67) Golovchenko, J. A.; Patel, J. R.; Kaplan, D. R.; Cowan, P. L.; Bedzyk, M. J. Solution to the Surface Registration Problem Using X-ray Standing Waves. *Phys. Rev. Lett.* **1982**, *49*, 560–563.

(68) Woodruff, D. P. Normal Incidence X-ray Standing Wave Determination of Adsorbate Structures. *Prog. Surf. Sci.* **1998**, *57*, 1–60.

(69) Blowey, P. J.; Rochford, L. A.; Duncan, D. A.; Warr, D. A.; Lee, T.-L.; Woodruff, D. P.; Costantini, G. Probing the Interplay Between Geometric and Electronic Structure in a Two-Dimensional K-TCNQ Charge Transfer Network. *Faraday Discuss.* **2017**, *204*, 97–110.

(70) Bartels, L.; Meyer, G.; Rieder, K.-H.; Velic, D.; Knoesel, E.; Hotzel, A.; Wolf, M.; Ertl, G. Dynamics of Electron-Induced Manipulation of Individual CO Molecules on Cu(111). *Phys. Rev. Lett.* **1998**, *80*, 2004–2007.

(71) Jelínek, P. High Resolution SPM Imaging of Organic Molecules with Functionalized Tips. *J. Phys. Cond. Matter* **2017**, *29*, 343002.

(72) Heinrich, B. W.; Iacovita, C.; Brumme, T.; Choi, D.-J.; Limot, L.; Rastei, M. V.; Hofer, W. A.; Kortus, J.; Bucher, J.-P. Direct Observation of the Tunneling Channels of a Chemisorbed Molecule. *J. Phys. Chem. Lett.* **2010**, *1*, 1517–1523.

(73) Rai, B. K.; Durbin, S. M.; Prohofsky, E. W.; Sage, J. T.; Wyllie, G. R.A.; Scheidt, W. R.; Sturhahn, W.; Alp, E. E. Iron Normal Mode Dynamics in (Nitrosyl)iron(II)tetraphenylporphyrin from X-ray Nuclear Resonance Data. *Biophys. J.* **2002**, *82*, 2951–2963.

(74) Gross, L.; Moll, N.; Mohn, F.; Curioni, A.; Meyer, G.; Hanke, F.; Persson, M. High-Resolution Molecular Orbital Imaging Using a p-Wave STM Tip. *Phys. Rev. Lett.* **2011**, *107*, 86101.

(75) Auwärter, W.; Seufert, K.; Klappenberger, F.; Reichert, J.; Weber-Bargioni, A.; Verdini, A.; Cvetko, D.; Dell'Angela, M.; Floreano, L.; Cossaro, A. *et al.* Site-Specific Electronic and Geometric Interface Structure of Co-Tetraphenyl-Porphyrin Layers on Ag(111). *Phys. Rev. B* **2010**, *81*, 245403.

(76) Weber-Bargioni, A.; Auwärter, W.; Klappenberger, F.; Reichert, J.; Lefrançois, S.; Strunskus, T.; Wöll, C.; Schiffrin, A.; Pennec, Y.; Barth, J. V. Visualizing the Frontier Orbitals of a Conformationally Adapted Metalloporphyrin. *Chem. Phys. Chem.* **2008**, *9*, 89–94.

(77) Schwarz, M.; Riss, A.; Garnica, M.; Ducke, J.; Deimel, P. S.; Duncan, D. A.; Thakur, P. K.; Lee, T.-L.; Seitsonen, A. P.; Barth, J. V. *et al.* Corrugation in the Weakly Interacting Hexagonal-BN/Cu(111) System: Structure Determination by Combining Noncontact Atomic Force Microscopy and X-ray Standing Waves. *ACS Nano* **2017**, *11*, 9151–9161.

(78) Mercurio, G.; Maurer, R. J.; Liu, W.; Hagen, S.; Leyssner, F.; Tegeder, P.; Meyer, J.; Tkatchenko, A.; Soubatch, S.; Reuter, K. *et al.* Quantification of Finite-Temperature Effects on

Adsorption Geometries of π-Conjugated Molecules: Azobenzene/Ag(111). *Phys. Rev. B* **2013**, *88*, 35421.

(79) Snezhkova, O.; Lüder, J.; Wiengarten, A.; Burema, S. R.; Bischoff, F.; He, Y.; Rusz, J.; Knudsen, J.; Bocquet, M.-L.; Seufert, K. *et al.* Nature of the Bias-Dependent Symmetry Reduction of Iron Phthalocyanine on Cu(111). *Phys. Rev. B* **2015**, *92*, 75428.

(80) Donovan, P.; Robin, A.; Dyer, M. S.; Persson, M.; Raval, R. Unexpected Deformations Induced by Surface Interaction and Chiral Self-Assembly of Co(II)-Tetraphenylporphyrin (Co-TPP) Adsorbed on Cu(110): A Combined STM and Periodic DFT Study. *Chem. - Eur. J.* **2010**, *16*, 11641–11652.

(81) Wagner, C. D.; Riggs, W. M.; Davis, L. E.; Moulder, J. F.; Muilenberg, G. E. *Handbook of X-ray Photoelectron Spectroscopy: A Reference Book of Standard Data for Use in X-ray Photoelectron Spectroscopy*; Perkin-Elmer Corp., Physical Electronics Division: Eden Prairie, MN, 1979.

(82) Wiengarten, A.; Seufert, K.; Auwärter, W.; Écija, D.; Diller, K.; Allegretti, F.; Bischoff, F.; Fischer, S.; Duncan, D. A.; Papageorgiou, A. C. *et al.* Surface-Assisted Dehydrogenative Homocoupling of Porphine Molecules. *J. Am. Chem. Soc.* **2014**, *136*, 9346–9354.

(83) Hieringer, W.; Flechtner, K.; Kretschmann, A.; Seufert, K.; Auwärter, W.; Barth, J. V.; Görling, A.; Steinrück, H.-P.; Gottfried, J. M. The Surface Trans Effect: Influence of Axial Ligands on the Surface Chemical Bonds of Adsorbed Metalloporphyrins. *J. Am. Chem. Soc.* **2011**, *133*, 6206–6222.

(84) Zhang, Q.; Kuang, G.; Pang, R.; Shi, X.; Lin, N. Switching Molecular Kondo Effect via Supramolecular Interaction. *ACS Nano* **2015**, *9*, 12521–12528.

(85) Chen, X.; Alouani, M. Effect of Metallic Surfaces on the Electronic Structure, Magnetism, and Transport Properties of Co-Phthalocyanine Molecules. *Phys. Rev. B* **2010**, *82*, 94443.

(86) Annese, E.; Fujii, J.; Vobornik, I.; Rossi, G. Structure and Electron States of Co-Phthalocyanine Interacting With the Cu(111) Surface. *J. Phys. Chem. C* **2011**, *115*, 17409–17416.

(87) Houwaart, T.; Le Bahers, T.; Sautet, P.; Auwärter, W.; Seufert, K.; Barth, J. V.; Bocquet, M.-L. Scrutinizing Individual CoTPP Molecule Adsorbed on Coinage Metal Surfaces from the Interplay of STM Experiment and Theory. *Surf. Sci.* **2015**, *635*, 108–114.

(88) Seufert, K.; Bocquet, M.-L.; Auwärter, W.; Weber-Bargioni, A.; Reichert, J.; Lorente, N.; Barth, J. V. Cis-Dicarbonyl Binding at Cobalt and Iron Porphyrins with Saddle-Shape Conformation. *Nat. Chem.* **2011**, *3*, 114–119.

(89) Buchner, F.; Kellner, I.; Hieringer, W.; Gorling, A.; Steinrück, H.-P.; Marbach, H. Ordering Aspects and Intramolecular Conformation of Tetraphenylporphyrins on Ag(111). *Phys. Chem. Chem. Phys.* **2010**, *12*, 13082–13090.

TOC Image